Beam Test of a Prototype Detector Array for the PoGO Astronomical Hard X-Ray/Soft Gamma-Ray Polarimeter

T. Mizuno *, T. Kamae, J. S. T. Ng and H. Tajima

Stanford Linear Accelerator Center, Menlo Park, California, 94025, USA

J. W. Mitchell and R. Streitmatter

NASA Goddard Space Flight Center, Greenbelt, Maryland, 20771, USA

R. C. Fernholz and E. Groth

Princeton University, Princeton, New Jersey, 08544, USA

Y. Fukazawa

Hiroshima University, Higashi-Hiroshima, Hiroshima, 739-8526, Japan

Abstract

Polarization measurements in the X-ray and gamma-ray energy range can provide crucial information on massive compact objects such as black holes and neutron stars. The Polarized Gamma-ray Observer (PoGO) is a new balloon-borne instrument designed to measure polarization from astrophysical objects in the 30-100 keV range, under development by an international collaboration with members from United States, Japan, Sweden and France. To examine PoGO's capability, a beam test of a simplified prototype detector array was conducted at the Argonne National Laboratory Advanced Photon Source. The detector array consisted of seven plastic scintillators, and was irradiated by polarized photon beams at 60, 73, and 83 keV. The data showed a clear polarization signal, with a measured modulation factor of 0.42 ± 0.01. This was successfully reproduced at the 10% level by the computer simulation package Geant4 after modifications to its implementation of polarized Compton/Rayleigh scattering. Details of the beam test and the validation of the Geant4 simulations are presented.

Key words: Polarimetry, Balloon, Gamma-ray, Monte Carlo
PACS: 95.55.Q

1 Introduction

Measurements of X-ray and gamma-ray polarization are expected to yield important information on a wide variety of astrophysical sources such as isolated pulsars, jet-dominated active galaxies, and accreting black holes and neutron stars. In the astrophysical environment, polarization arises under a variety of conditions. Polarization in synchrotron radiation is due to the electrons gyrating in ordered magnetic fields [1], providing information on the properties of magnetic fields around the source. The absorption cross-section of photons, as they propagate through a strong magnetic field, is polarization and energy dependent, making it possible to investigate the strong-field environment near the surface of a neutron star [2,3]. Polarization can also result from the Compton scattering of an incident photon flux in the accretion disks around compact stars and active galactic nucleus. In all cases, the orientation of the polarization plane depends on the orientations of the magnetic fields and the accretion disk, hence it is a powerful probe of the source geometry. However, despite its importance, X-ray and gamma-ray polarization has been measured by only two experiments, one on the OSO-8 satellite which viewed the Crab at 2.6 and 5.2 keV and measured the polarization using Bragg diffraction [4–6], the other on the RHESSI satellite which has reported the detection of polarization for a gamma-ray burst [7]. Thus far, there has been no systematic study of polarization in high-energy astrophysics due to the lack of sensitivity, and polarization at hard X-ray and soft gamma-ray energies, where non-thermal processes are likely to produce a high degree of polarization, is yet to be explored. We note that, on the other hand, there has been a long history of attempts to measure polarization of hard X-rays in solar flares followed by recent missions of SPR-N on CORONAS-F [8] and RHESSI [9]. See an introduction section in [9] and references therein for a review.

To carry out these measurements, we are constructing a new balloon-borne instrument, the Polarized Gamma-ray Observer (PoGO), which employs coincident detection of Compton scattering and photo-absorption to measure polarization in the 30–100 keV energy range. The PoGO instrument utilizes an adaption to polarization measurements of the well-type phoswich counter design developed through a series of balloon experiments [10–16] and implemented in the ASTRO-E/ASTRO-E2 satellite mission as the Hard X-ray Detector [17–20]. Through these balloon experiments and tests on the ground, the well-type phoswich counter design has been shown to be highly effective in reducing background and has achieved high sensitivity in measuring hard X-ray spectra [10,16,17,19]. The conceptual design of the PoGO instrument is shown in Figure 1. A hexagonal array of fast plastic scintillators function

* Corresponding author. Tel.:+1-650-926-2595, fax.:+1-650-926-4979.
Email address: mizuno@SLAC.Stanford.EDU

as a Compton polarimeter for hard X-rays/soft gamma-rays by measuring the azimuthal scattering angle asymmetry. This is surrounded by bottom and side anti-coincidence detectors made of bismuth germanate oxide (BGO) scintillators. The aperture is defined by active collimators made from tubes of slow plastic scintillator. A similar modular polarimeter can be found as GRAPE [21,22], which is optimized for measuring polarization of energy $\geq$ 100 keV from solar flares and gamma-ray bursts.

To simplify readout, the instrument is organized as an array of hexagonal phoswich units, each consisting of a fast scintillator (decay time $\tau \sim 2$ ns), a slow plastic scintillator active collimator ($\tau \sim 300$ ns), and a bottom BGO anti-coincidence detector ($\tau \sim 300$ ns), all viewed by a single photomultiplier tube (PMT). In order to reduce the background due to downward atmospheric gammas and cosmic diffuse gammas coming from outside the field-of-view, we also use a thin high-Z metal foil, wrapped around the active collimator tubes, as passive collimators. Signals from the fast plastic scintillator and those from the slow plastic or BGO scintillator can be separated using a pulse shape discrimination technique by examining signal development in two different time windows.

The design parameters of PoGO, and its expected performance and response to polarized gamma-rays have been studied in extensive Monte-Carlo simulations using the EGS4 [23] and Geant4 [24] computer program packages. The current design of PoGO consists of 217 phoswich units composed of 3 cm long BGO scintillator, 20 cm long fast scintillator and 60 cm long slow scintillator, each one is of $\sim$2.6 cm wide. The width is determined by the availability of PMTs with large photocathode area, and the length of fast scintillators is determined to maximize the sensitivity for polarization. Our initial study with Monte-Carlo simulation showed that the length of 15–20 cm could be optimum: Scintillators longer than photon attenuation length for the energy of our interest are preferred, since the forward scattered photons are still highly polarized, and hence events with double Compton scatterings in a scatterer scintillator exhibit high azimuthal scattering angle asymmetry (see also a discussion in § 3). A geometrical area is ~ 930 cm^2 and an effective area is ~ 230 cm^2 at 40 keV, when we require that two fast scintillators detect a hit with a threshold level of 3 keV to select Compton events. The Monte-Carlo simulations also show that PoGO will achieve the sensitivity to measure better than 10% polarization from a 100 mCrab source in a single 6 hour balloon observation. More details of the instrumentation can be found in [25].

2 Beam Test at the APS

To validate our simulations of polarized Compton scattering process, and to demonstrate the ability of PoGO to measure polarization, we have conducted a test-beam experiment with a PoGO prototype at the Advanced Photon Source Facility (APS) of the Argonne National Laboratory during November 10–18, 2003. Because the main objective of the beam test was to measure the sensitivity, in the energy regime of interest, of the PoGO technique of Compton polarimetry, the prototype only included the fast plastic scintillators. This simplified the read-out scheme, and we did not need to use the pulse shape discrimination technique. The prototype was arranged as an array of 7 hexagonal Saint-Gobain BC-404 scintillators, each 2.68 cm wide and 20 cm long, as shown in Figure 2 (which includes the numbering scheme). Each scintillator was glued directly to a Hamamatsu R580 PMT (3.4 cm photocathode diameter, larger than that of PMTs used for PoGO flight). The center scintillator acted as a Compton scattering target and the outer six scintillators, separated from the center scintillator by 2.2 cm, detected the scattered photons. In the final PoGO instrument the hexagonal detector units will be tightly bundled together in a close-packed hexagonal array [25]. However, photons scattered in one detector are likely to pass through at least its nearest neighbors before being photo-absorbed in other units. Thus, the prototype array approximates a region of the final PoGO instrument. Tests with slow scintillator collimators and bottom/side BGO scintillators and with larger number of units will be done in fiscal year of 2005 and 2006.

The experiment was installed in the MUCAT 6ID-D station, which enabled us to control (reduce) the beam intensity down to an appropriate flux for our instrument. The test detector was exposed to plane-polarized photon beams at 60 keV, 73 keV, and 83 keV delivered through an undulator and a double-scattering monochromator upstream. The beam line was operated in a reduced flux mode by detuning one stage of the monochromater with a typical flux of approximately 10^7 photons s^{-1}. This was further reduced with attenuators, resulting in a trigger rate of a few kHz at the experiment. The degree of polarization was calculated to be 98–99%; there was also the background (a non-polarized broad-band continuum and photons not associated with the beam) which contributed to approximately 2-3% of the flux.

The array was mounted on a rotation stage, as shown in Figure 3, to allow measurement of the modulation factor by rotating about the center scintillator aligned to the incident photon beam. To measure the detector response to various orientations of the polarization vector, the instrument was rotated in 15 degree steps covering the entire azimuthal angle range (0–360 degree). For each run, we integrated about 100k events. Data at the three different beam energies allowed for calibration of the detector, providing the energy vs.

pulse height scale factors as well as the energy resolution for each sensor. The calibration data were obtained by irradiating beam at each detector with a self trigger. The energy resolution (full width at half maximum) at 73 keV spanned the range of 25 % to 33 % and scaled with the inverse of the square-root of energy.

The signals from the PMT anodes were fed into charge-sensitive preamplifiers and then filtered and amplified by shaping amplifiers with 1 μs shaping time. The outputs of these amplifiers were used for both trigger generation and spectroscopy. A Compton scattering trigger was generated by a coincidence of hits in the central scintillator and in any one of the surrounding scintillators, with a threshold of about 0.5 keV and 5 keV, respectively. The data acquisition system is shown in Figure 4. Note that the electronic readout scheme is different from that of the final PoGO instrument [25].

During the experiment, we observed that the trigger efficiency varied among the peripheral scintillators. In order to evaluate this, we collected an unbiased data sample, at 73 keV for the angular range of 0–150 degree in 30 degree steps, triggered only by the central scintillator (channel 4). We applied the event selection criteria described in § 3 and calculated the trigger efficiency as the ratio of counts of coincidence trigger run to that of channel 4 trigger run for each peripheral scintillator. The relative efficiency was the highest for channel 7 (normalized to 1) and the lowest for channel 6 ($\sim$ 0.65); the efficiencies were determined with a statistical error of $\sim$2.5%. These were taken into account in the following analysis.

3 Data Analysis and Simulation

A raw data sample at 73 keV taken with coincidence trigger at 0-degree rotation is shown in Figure 5 as a scatter-plot of the energy detected in the central scintillator and the total energy detected in all seven scintillators. The strip structure at $\sim$ 10 keV energy deposition in the central scintillator was due to the trigger inefficiency mentioned in § 2. We can see a clear separation between events in which Compton scattered photons were photo-absorbed in the peripheral scintillators (total energy deposit at about 73 keV) and those in which the scattered photons escaped (total energy deposit below 40 keV). In order to select valid Compton events, i.e., events in which incident photon was Compton-scattered in the central scintillator and photo-absorbed in only one of the peripheral scintillators, we applied the following criteria: 1) the central scintillator and only one of the outside scintillators detected a hit, where detection threshold was set at 3 keV, well above the single photo-electron noise (corresponding to 1–1.5 keV energy deposition); 2) the energy detected in the central scintillator was below 40 keV and less than half of the total energy

deposit, to ensure that the central scintillator scattered the incident photon; and 3) the total energy deposit is 73.2 ± 25 keV, consistent with incident beam energy within detector energy resolution. The selection criteria are also shown in Figure 5. (Note that the surrounding slow plastic and BGO scintillators onboard the PoGO flight-instrument will allow us to eliminate events where the incident photon did not deposit its full energy in the fast scintillators, even without any information on the initial energy.) Polarization could then be determined by the variation in hit rates in each peripheral scintillator due to the anisotropy in the probability of azimuthal scattering angles of Compton events.

The results, taking variation in trigger efficiencies into account, are summarized in Figure 6. There, the average of counts of channels 1 and 7, that of channels 2 and 6, and that of channels 3 and 5 are plotted as a function of instrument rotation angle. We normalized the data to the number of selected events, since the total photon flux was not recorded. A clear modulation can be seen, with the least counts in scintillators along the polarization vector (e.g., channels 3 and 5 for 0-degree rotation) and the highest counts in those perpendicular to the vector as expected. We fit the result to a sinusoidal curve and obtained a modulation factor (M_p) from the maximum ($R_{\rm max}$) and minimum ($R_{\rm min}$) rates measured as a function of azimuthal angle by:

$$M_p = \frac{R_{\rm max} - R_{\rm min}}{R_{\rm max} + R_{\rm min}} \tag{1}$$

The resulting modulation factor of 0.421 ± 0.010 from the normalized data, is consistent with the value of 0.423 ± 0.012 obtained from the unbiased data sample taken with triggers in the central scintillator only. Similar event selections applied to the 60 keV and 83 keV data samples yielded a modulation factor of 0.402 ± 0.011 and 0.416 ± 0.010, respectively, indicating that the modulation factor is almost independent of the beam energy.

Our results were compared with computer simulations using the Geant4 toolkit (version 5.1) [24] with low energy extensions which are especially important for simulating polarized photon scattering. Initial simulations gave a modulation factor of ~ 0.37, resulting in an unphysical polarization value (over 100%). This was due to an incorrect implementation of the polarized Compton and Rayleigh scattering processes in the code. As described in detail in Appendix A, we improved it and validated it against another simulation program EGS4 [23,26,27]. Note that Geant4 provides greater flexibility in simulating complex geometries compared to other codes such as EGS4; therefore it is more suitable for studying the response of a complicated instrument such as PoGO.

The new Geant4 simulator yielded a modulation factor of 0.488 ± 0.006 for a

fully-polarized 73 keV photon beam and a perfectly aligned PoGO prototype detector. By taking into account the degree of polarization of the beam and the effect of the background, we obtained a modulation factor of about 0.47. The small (10%) difference from the data could be accounted for by the uncertainty of the simulation (see Appendix A) and possibly by misalignment of the instrument. Simulations for photon beams at 60 keV and 83 keV yielded consistent modulation factors of 0.487 ± 0.006 and 0.489 ± 0.008, respectively. The small (~ 4 %) energy dependence seen in data could be due to the energy dependence of the trigger efficiency.

Since the PoGO scintillators are much longer than the photon attenuation length at the test beam energies (~ 6 cm), the probability of double scattering in one scintillator is not negligible. About $\frac{1}{3}$ of the events that passed the selection criteria showed energy depositions of more than 15 keV in the central scintillator (corresponding to a scattering angle of 150°), consistent with double scattering. Even for these events, data collected using triggers with central scintillator hit only yielded a moderately high modulation factor of 0.285 ± 0.022, indicating that our crude event selection resulted in moderate modulation factors as well as high photon statistics. This would be an advantage in astrophysical observations with limited photon statistics.

4 Summary

We have conducted a beam test experiment on a prototype of the Polarized Gamma-ray Observer (PoGO), under development for polarization studies of high-energy astrophysics processes in the hard X-ray/soft gamma-ray regime. The prototype consisted of seven plastic scintillators read out with PMTs, and was exposed to polarized photon beams at 60 keV, 73 keV and 83 keV. We obtained a clear modulation signal with a measured modulation factor of 0.42 ± 0.01. We also compared our results with the Geant4 simulation program and found that its implementation of polarized Compton/Rayleigh scattering processes required modifications. The modified Geant4 simulation results agreed with our data to 10%. The new Geant4 was also validated against EGS4 at the 2–3% level.

5 Acknowledgement

This work was partially supported by the U.S. Department of Energy under contract DE-AC03-76SF00515 and NASA under RTOP 187-01-01-07. We would like to thank the APS staff for their generous and friendly support, in

particular D. Robinson whose help made possible the success of this experiment. We are also grateful to members of PoGO collaboration. In particular, we would like to thank J. Kataoka, Y. Yatsu, T. Ikagawa, Y. Yamashita and M .Suhonen for their support for the experiment at Spring-8, which was indispensable for the success of this experiment. We would also like to thank D. Marlow, G. Bogaert, T. Thurston, A. Scholz and R. Rogers for their support for the test preparation. Use of Advanced Photon Source was supported by the U. S. Department of Energy, Basic Energy Science, Office of Science, under Contract No. W-31-109-Eng38.

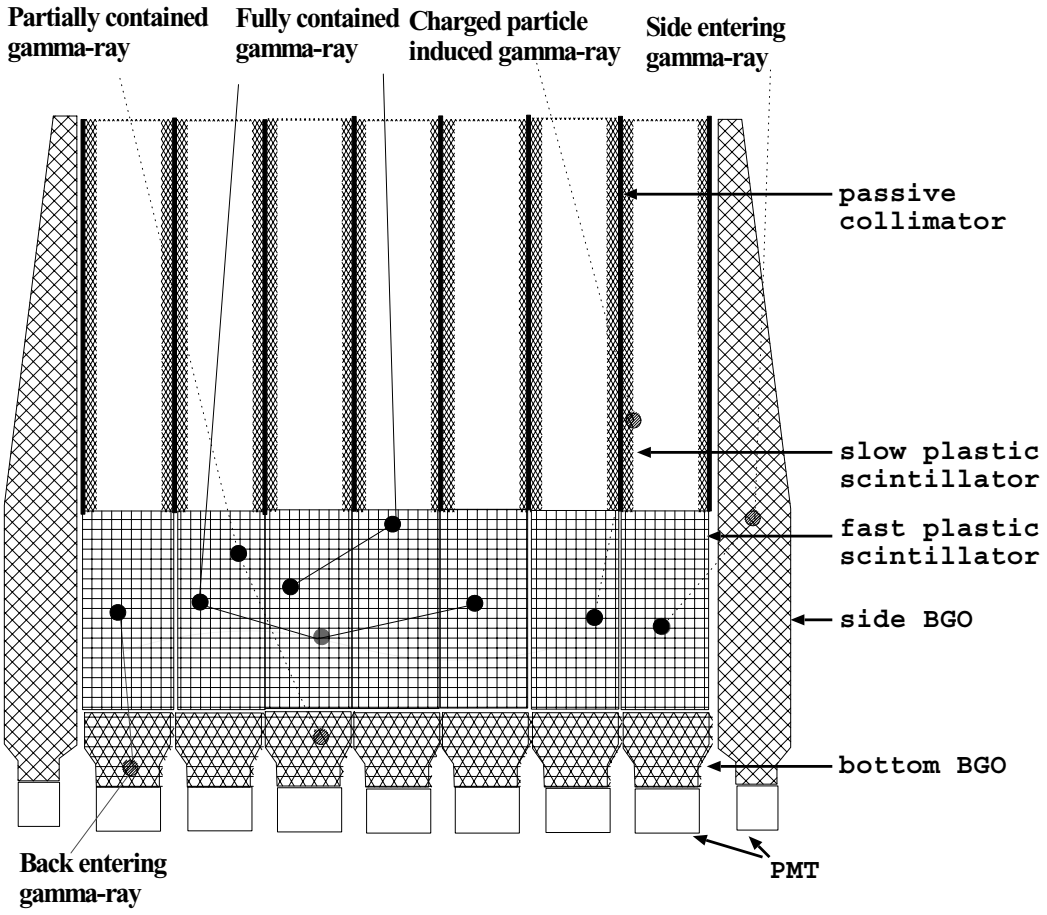

Fig. 1. Conceptual design of PoGO. It consists of an array of well-type phoswich detector units, each made of a fast plastic scintillator, a slow plastic scintillator tube, a thin high-Z metal foil and a bottom BGO. A set of side anti-coincidence detectors made of BGO surrounds the array of phoswich units. In the figure, representative passages of gamma-rays are shown with energy deposition marked by circles. The trigger scheme accepts only the ones marked as "Fully contained gamma-ray".

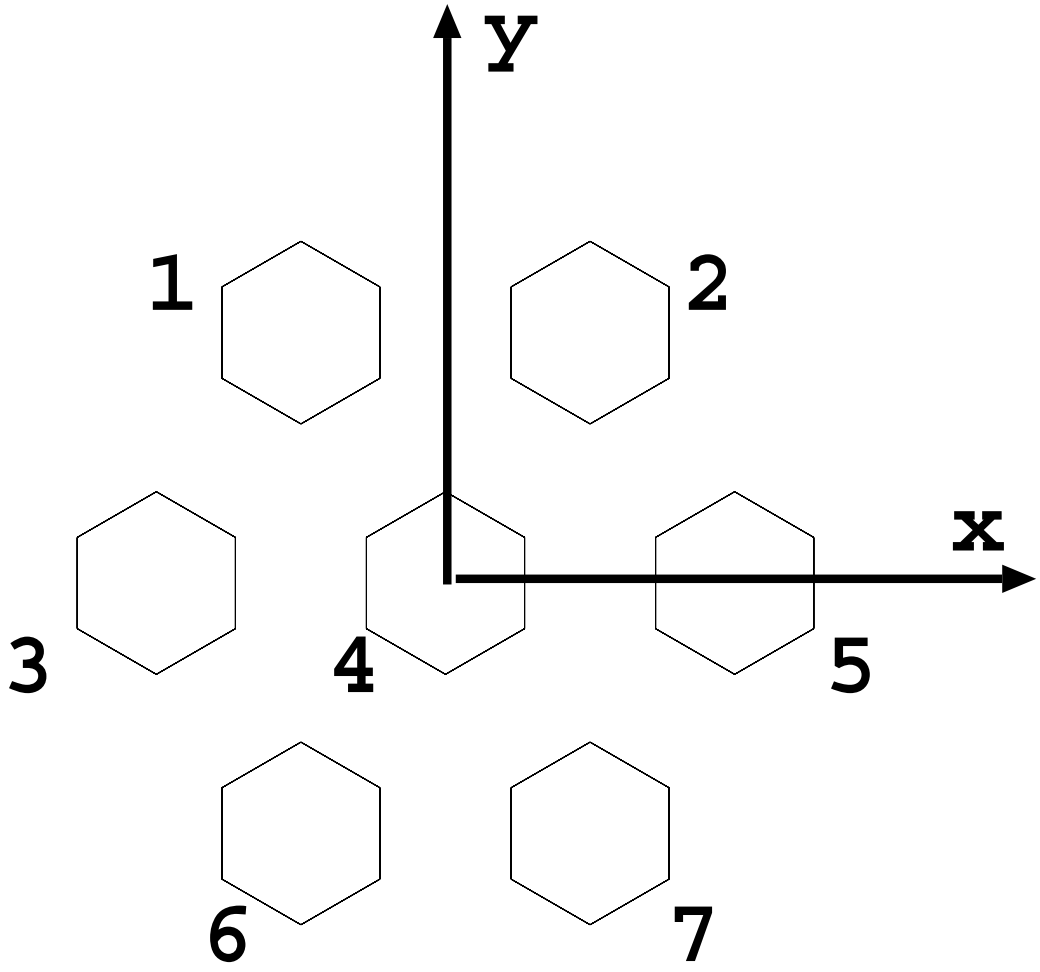

Fig. 2. The layout and numbering scheme of scintillators viewed from the beam origin. Detector rotation angle is defined to be 0° when scintillators channels 3, 4 and 5 are along the horizontal (x-axis), and to be 30° when channels 1, 4 anc 7 are along the vertical (y-axis).

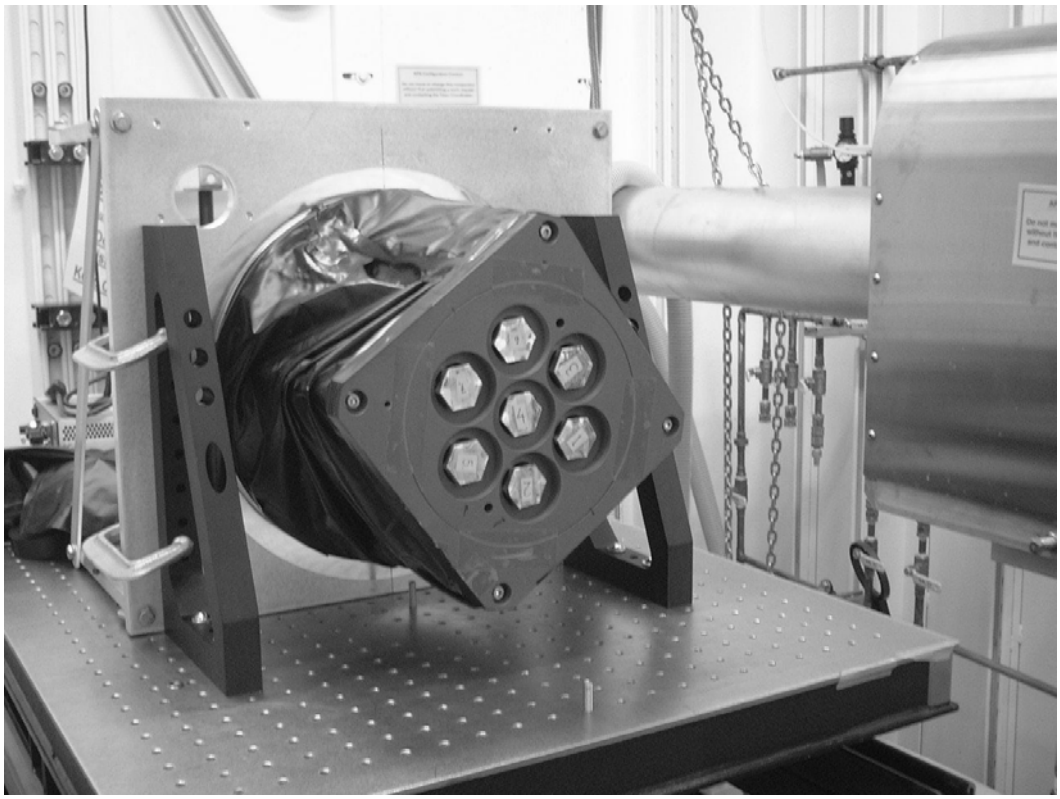

Fig. 3. A photograph of the PoGO prototype mounted on the rotation stage attached to the experiment table.

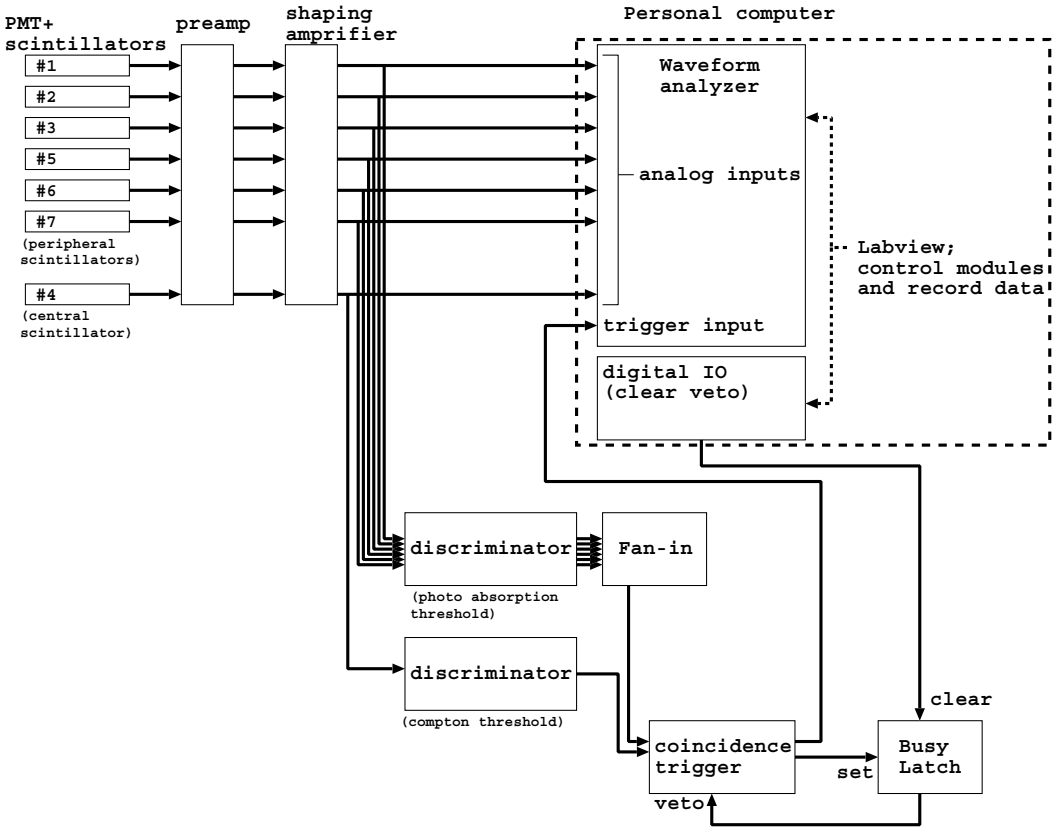

Fig. 4. The data acquisition system of the experiment. Outputs from shaping amplifiers are used for trigger generation and spectroscopy; the trigger was generated by a coincidence of hits in the central scintillator and in any one of the peripheral scintillators.

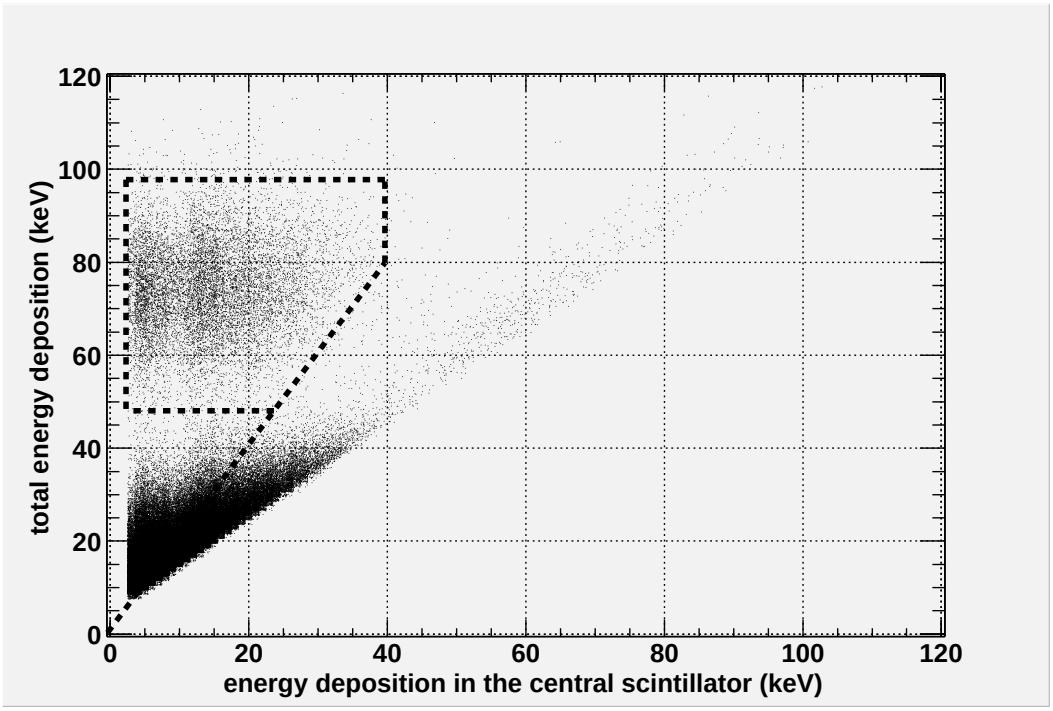

Fig. 5. Relation of deposit energy in the central scintillator and total energy deposition for 73 keV run at 0-degree rotation. Event selection criteria used in data analysis are also shown by dotted lines. (see text)

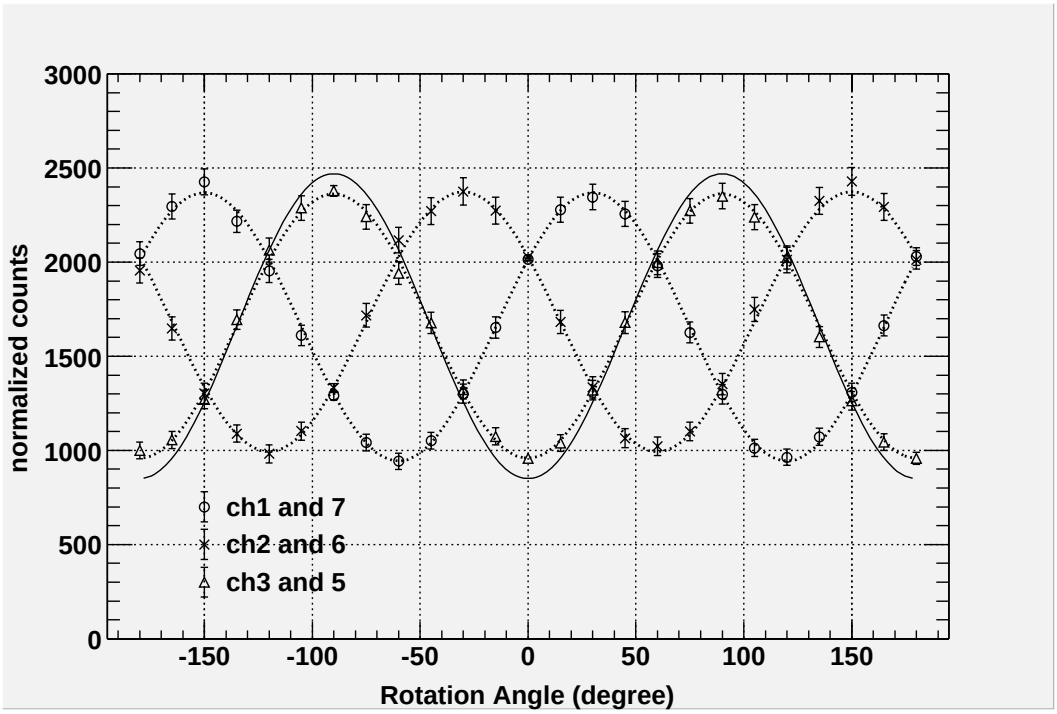

Fig. 6. Normalized counts in peripheral scintillators as a function of rotation angle for 73 keV run. Best fit models are given as dotted lines. For channels 3 and 5, the prediction by Geant4 (with modifications; see text) for 100% linearly polarized beam is shown by thin solid line.

A Geant4 Simulation of Polarized Photon Scattering

Geant4 [24] is a toolkit for simulating the passage of particles through matter. It has now become a standard tool in a wide variety of fields, e.g., high energy physics, medical science, astrophysics and space science. It simulates a comprehensive range of physical processes including electromagnetic, hadronic and optical interactions and facilitates handling of complex geometries in the simulation. It is, however, a relatively new product (the first public release was in December 1998) and needs to be validated by comparison with experimental data, theoretical predictions and other simulation programs.

To reproduce our beam test data, we used Geant4 with the low energy extensions (G4LowEnergyPolarizedCompton class [28] and a G4LowEnergyRayleigh class) for photon scattering simulations. We used version 5.1 and confirmed that the classes had not been changed over versions 4.2–6.2 with regard to the polarized photon scattering. Initial simulations gave a modulation factor of ~ 0.37, implying an unphysical beam polarization of over 100%. We examined the Geant4 simulation program in detail and found that even for the forward scattering case, in which energy transfer is negligible and a scattered photon is expected to remain $\sim 100\%$ linearly polarized, the polarization vector after the scattering changed to some degree (Figure A1). We also noticed that the Rayleigh scattering extinguished the photon polarization vector, and consequently gave an artificially small modulation. We therefore had to modify the implementation of polarized Compton/Rayleigh scattering in Geant4 as described below.

The notation is defined as in Figure A2. There, one completely linearly polarized photon is scattered by a free electron at point O. The momentum vector of incident and scattered photon are $\vec{k_0}$ and $\vec{k}$, respectively, and the unit vector along the polarization vector before the scattering is $\vec{e_0}$. θ and ϕ are the polar and azimuth angle of the scattering. Here, $\vec{k_0}$ and $\vec{e_0}$ are assumed to be along z-axis and x-axis, respectively. Then, the Klein-Nishina cross section of the Compton scattering is given by

$$\frac{d\sigma}{d\Omega} = \frac{1}{2} {r_0}^2 \frac{k^2}{{k_0}^2} \left[\frac{k}{k_0} + \frac{k_0}{k} - 2\sin^2\theta\cos^2\phi \right] \quad , \tag{A.1}$$

and the Thomson scattering cross section is, by substituting k_0 for k, given by

$$\frac{d\sigma}{d\Omega} = {r_0}^2 \left(1 - \sin^2\theta\cos^2\phi\right) \quad . \tag{A.2}$$

We can see that photons are most likely scattered at right angle to the direction of incident polarization vector ($\phi = 90^\circ$). If we use the angle between the

incident polarization vector ($\vec{e_0}$) and the scattered polarization vector $\vec{e}$, the formula can also be expressed as

$$\frac{d\sigma}{d\Omega} = \frac{1}{4}{r_0}^2 \frac{k^2}{{k_0}^2}\left[\frac{k}{k_0} + \frac{k_0}{k} - 2 + 4\cos^4\Theta\right] \tag{A.3}$$

and

$$\frac{d\sigma}{d\Omega} = {r_0}^2 \cos^4\Theta \tag{A.4}$$

for the Compton and Thomson scattering, respectively, where Θ is the angle between two polarization vectors [29]. The cross section per atom is obtained by taking into account the incoherent scattering function (for the Compton scattering) or the atomic form factor (for the Rayleigh scattering) [30,31].

According to [29], it is convenient to consider two directions for $\vec{e}$: one is in the same plane as $\vec{e_0}$ (denoted as $\vec{e_\parallel}$) and the other is perpendicular to it ($\vec{e_\perp}$). Then, the differential cross section for these two directions is

$$\left(\frac{d\sigma}{d\Omega}\right)_\parallel = \frac{1}{4}{r_0}^2 \frac{k^2}{{k_0}^2}\left[\frac{k}{k_0} + \frac{k_0}{k} - 2 + 4\left(1 - \sin^2\theta\cos^2\phi\right)\right] \ , \tag{A.5}$$

and

$$\left(\frac{d\sigma}{d\Omega}\right)_\perp = \frac{1}{4}{r_0}^2 \frac{k^2}{{k_0}^2}\left[\frac{k}{k_0} + \frac{k_0}{k} - 2\right] \ . \tag{A.6}$$

The cross sections for the Thomson scattering is obtained by substituting k_0 for k. Then we obtain $\left(\frac{d\sigma}{d\Omega}\right)_\perp = 0$ and can see that the scattered photon is linearly polarized along $\vec{e_\parallel}$. For the Compton scattering case, a scattered photon is partially polarized along $\vec{e_\parallel}$ and the degree of polarization is calculated from the maximum and minimum values of the cross section ($\left(\frac{d\sigma}{d\Omega}\right)_\parallel$ and $\left(\frac{d\sigma}{d\Omega}\right)_\perp$, respectively) as [1]

$$P \equiv \frac{\left(\frac{d\sigma}{d\Omega}\right)_\parallel - \left(\frac{d\sigma}{d\Omega}\right)_\perp}{\left(\frac{d\sigma}{d\Omega}\right)_\parallel + \left(\frac{d\sigma}{d\Omega}\right)_\perp} = \frac{2\left(1 - \sin^2\theta\cos^2\phi\right)}{\frac{k}{k_0} + \frac{k_0}{k} - 2\sin^2\theta\cos^2\phi} \ . \tag{A.7}$$

On the other hand, when the scattered photon is depolarized with a probability of $1 - P$, we sampled the direction of polarization vector at random in the plane constructed by $\vec{e_\parallel}$ and $\vec{e_\perp}$. Except for the way of sampling the polarization vector, we used the original code for low-energy Compton/Rayleigh

scattering. The distribution of the polarization vector after Compton scattering in forward direction, obtained by simulation with the new codes, is also shown in Figure A1. We note that the way of sampling the polarization vector is identical with that of EGS4 with polarized photon scattering as described in [26]; we have not implemented Doppler broadening yet [27].

We validated the Geant4 simulation with our modifications in detail by comparing with the results of EGS4 simulation which included the effects of Compton and Rayleigh scattering for polarized gamma-rays and the effect of Doppler broadening [26,27]. The EGS4 program had been validated at the $\sim 10\%$ level by comparing with polarization measurements [26]. In our validation test, we simulated a slab of 20 cm thick plastic scintillator and irradiated it with 5 million photons (100% linearly polarized) with a power-law energy spectrum with an index of 2.1 to mimic the Crab Nebula spectrum in 25–200 keV energy range [32]. Azimuthal angle asymmetry of the first and the second Compton scattering are summarized in Figure A3. There, the distribution of Geant4 results with and without our modifications are compared with EGS4 results. Distributions of the first Compton scattering are almost identical between EGS4 and the modified Geant4, giving a modulation factor of 0.4941 ± 0.0006, whereas the original Geant4 shows a smaller value of 0.4653 ± 0.0006 due to the (incorrect) Rayleigh scattering depolarization effect. For the second Compton scattering, EGS4 and the new Geant4 again give a consistent modulation factor (0.3248 ± 0.0008). On the other hand, the original Geant4 shows a much less isotropic distribution (modulation factor of only 0.1669 ± 0.0008) due to the implementation problems already mentioned.

Finally, as an overall validation of polarized scattering processes, we compared an expected modulation factor of the PoGO instrument predicted by three simulation programs. To do this we segmented hits in the plastic slab into hexagonal elements of 2.68 cm thickness (current design value of PoGO) and incorporated a typical PMT noise and the energy resolution of the scintillators. The obtained modulation factor was 0.2184 ± 0.0022 and 0.2223 ± 0.0023 for EGS4 and modified Geant4, respectively, whereas that by original Geant4 was 0.1239 ± 0.0023 (Figure A4). We therefore conclude that the modified Geant4 and EGS4 are consistent in 2–3% level when applied to simulating PoGO with polarized Compton/Rayleigh scattering. This study has already been reported to Geant4 team, and new codes will be available in the public release after the test is done.

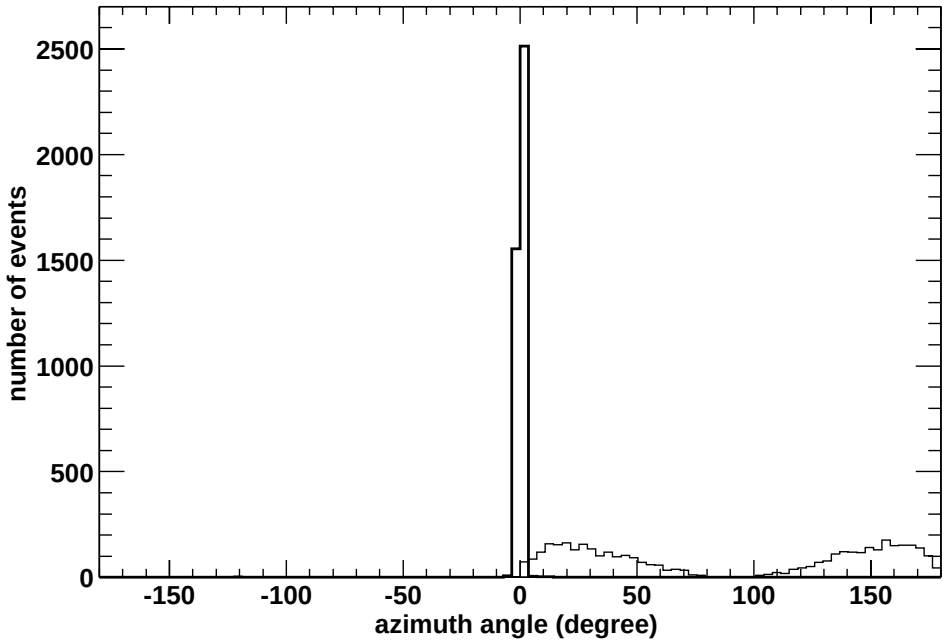

Fig. A.1. Azimuthal angle distribution of the polarization vector of 100% linearly polarized photons, after the first Compton scattering. Beam energy is 100 keV and forward scattering events ($\cos\theta \geq 0.95$) are selected. Distribution obtained by original Geant4 codes is given by thin solid line and that with our fixes by thick one. The vector is parallel to the initial beam polarization vector when the angle is 0°.

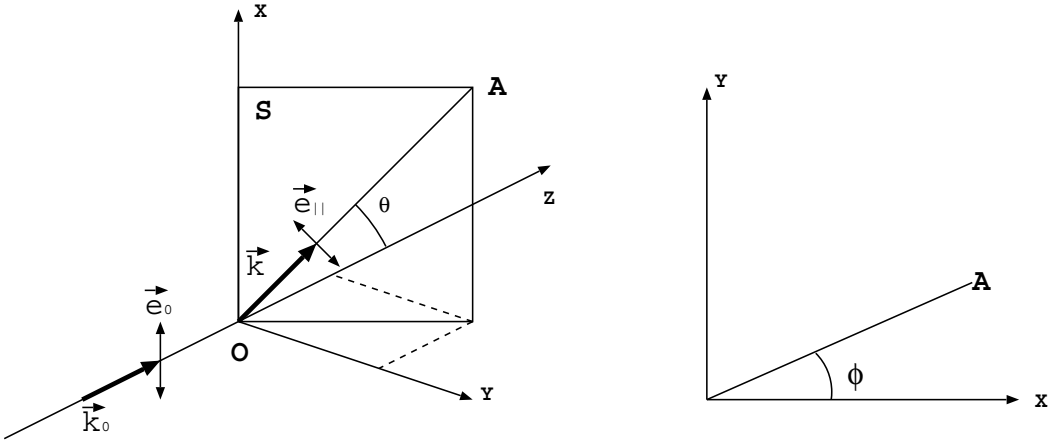

Fig. A.2. A photon scattering at point O. The momentum vector ($\vec{k_0}$) and the polarization vector ($\vec{e_0}$) of an incident photon are along z- and x-axis, respectively. θ and ϕ are the scattering polar and azimuth angle. Plane S is constructed by $\vec{e_0}$ and $\vec{k}$, the momentum vector after the scattering. $\vec{e_\parallel}$ is in plane S.

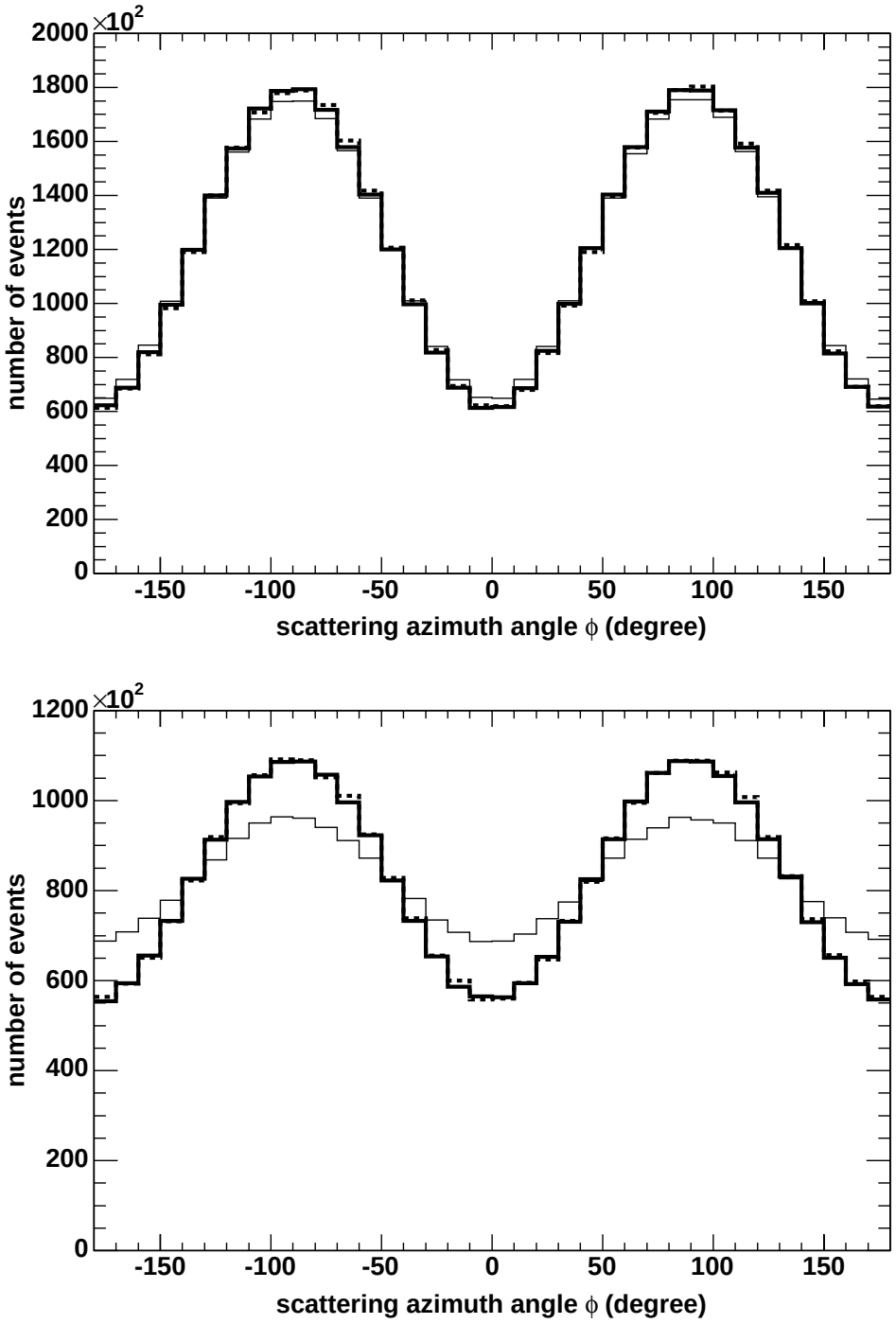

Fig. A.3. Azimuthal angle asymmetry of the first (top panel) and the second (bottom panel) Compton scattering for the fully polarized Crab spectrum in 25–200 keV, where the angle is measured from the polarization vector of the incident photon. The distribution of modified Geant4, original Geant4 and EGS4 (all with polarized Compton scattering process) are shown by thick solid line, thin solid one and dotted line, respectively. For Geant4 with our fixes and EGS4 simulation, polarized Rayleigh scattering is also implemented.

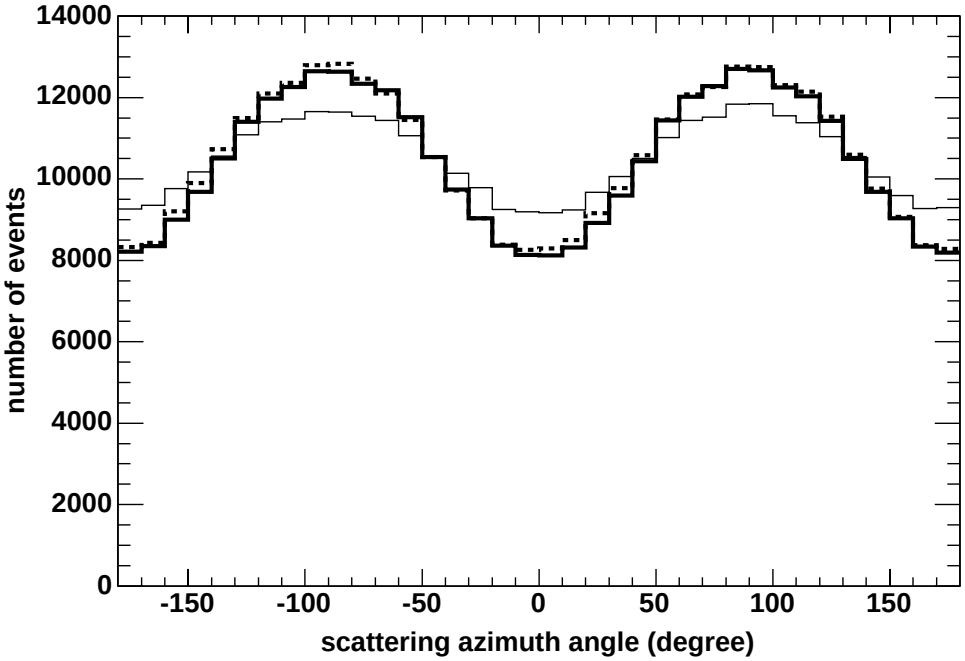

Fig. A.4. Predicted azimuthal angle distribution of the Crab Nebula spectrum observed by the PoGO instrument. Like for Figure A3, the predictions by modified Geant4, original Geant4 and EGS4 are shown by thick solid line, thin solid one and dotted line, respectively.

References

[1] G. B. Rybicki and A. P. Lightman, Radiative Processes in Astrophysics, John Wiley & Sons, New York, 1979

[2] A. K. Harding, Science 251 (1991) 1033.

[3] A. K. Harding, Physics Reports 206 (1991) 327.

[4] M. C. Weisskopf, G. G. Cohen, H. L. Kestentaum, K. S. Long, R. Novick, and R. S. Wolef, Astrophysical Journal 208 (1976) L125.

[5] M. C. Weisskopf, E. H. Silver, H. L. Kestenbaum, K. S. Long, and R. Novick, Astrophysical Journal 220 (1978) L117.

[6] E. H. Silver, M. C. Weisskopf, H. L. Kestenbaum, K. S. Long, R. Novix, and R. S. Wolef, Astrophysical Journal 225 (1978) 221.

[7] W. Coburn and S. Boggs, Nature 423 (2003) 415.

[8] A. V. Bogomolov et al., Solar System Research 37 (2003) 112.

[9] M. L. McConnell, D. M. Smith, A. G. Emslie, G. J. Hurford, R. P. Lin and J. M. Ryan, Advances in Space Research 34 (2004) 462.

[10] S. Gunji et al., Astrophysical Journal 397 (1992) L83.

[11] S. Gunji et al., Astrophysical Journal 428 (1994) 284.

[12] S. Miyazaki et al., Pub. Astron. Soc. Japan 48 (1996) 801.

[13] N. Yamasaki et al., Astrophysical Journal 481 (1997) 821.

[14] T. Kamae et al., proc. SPIE 1734 (1992) 2.

[15] T. Kamae et al., IEEE Trans. Nucl. Sci. 40(2) (1993) 204.

[16] T. Takahashi et al., IEEE Trans. Nucl. Sci. 40(4) (1993) 890.

[17] T. Kamae et al., proc. SPIE 2806 (1996) 314.

[18] T. Takahashi et al., Astronomy and Astrophysics Supplement 120 (1996) 645.

[19] C. Tanihata et al., proc. SPIE 3765 (1999) 645.

[20] K. Makishima et al., A. S. P Conf. Proc. 251, ed. H. Inoue and H. Kunieda, Astr. Soc. of the Pacific (2001) 564.

[21] M. L. McConnell, J. R. Macri, M. McClish, J. Ryan, D. J. Forrest and W. T. Vestrand, IEEE Trans. Nucl. Sci. 46(4) (1999) 890.

[22] M. L. McConnell, J. Ledoux, J. R. Macri and J. Ryan, proc. SPIE 5165 (2004) 334.

[23] W. R. Nelson, H. Hirayama and D. W. O. Rogers, SLAC-Report 265 (1985).

[24] S. Agostinelli et al., Nucl. Instr. and Meth. A 506 (2003) 250.

[25] P. Chen et al., in Proc. IEEE Nuclear Science Symp., Portland, Oregon, October 2003

[26] Y. Namito, S. Ban and H. Hirayama, Nucl. Instr. and Meth. A 332 (1993) 277.

[27] Y. Namito, S. Ban and H. Hirayama, Nucl. Instr. and Meth. A 349 (1994) 489.

[28] G. O. Depaola, Nucl. Instr. and Meth. A 512 (2003) 619.

[29] W. Heitler, The Quantum Theory of Radiation, Oxford Clarendom Press, 1954.

[30] J. H. Hubbell et al., J. Phys. Chem. Ref. Data 4 (1975) 471.

[31] J. H. Hubbell and I. Overbø, J. Phys. Chem. Ref. Data 9 (1979) 69.

[32] A. Toor and F. D. Seward, Astrophysical Journal 79 (1974) 995.